Article

Seasonal Variability in Fine Particulate Matter Water Content and Estimated pH over a Coastal Region in the Northeast Arabian Sea

Garima Shukla [1,2], A. K. Sudheer [3], Sachin S. Gunthe [4,5], Gufran Beig [6] and Ashwini Kumar [1,2,*]

[1] CSIR-National Institute of Oceanography, Dona Paula 403004, India
[2] Academy of Scientific and Innovative Research (AcSIR), Ghaziabad 201002, India
[3] Physical Research Laboratory, Department of Space, Ahmedabad 380009, India
[4] Environmental Engineering Division, Department of Civil Engineering,
   Indian Institute of Technology Madras, Chennai 600036, India
[5] Laboratory for Atmospheric and Climate Sciences, Indian Institute of Technology Madras,
   Chennai 600036, India
[6] National Institute of Advanced Studies, Indian Institute of Science Campus, Bangalore 560012, India
* Correspondence: ashwinik@nio.org; Tel.: +91-832-2450368; Fax: +91-832-2450602

Abstract: The acidity of atmospheric particles can promote specific chemical processes that result in the production of extra condensed phases from lesser volatile species (secondary fine particulate matter), change the optical and water absorption characteristics of particles, and enhance trace metal solubility that can function as essential nutrients in nutrient-limited environments. In this study, we present an estimated pH of fine particulate matter (FPM) through a thermodynamic model and assess its temporal variability over a coastal location in the northeast Arabian Sea. Here, we have used the chemical composition of FPM ($PM_{2.5}$) collected during the period between 2017–2019. Chemical composition data showed large variability in water-soluble ionic concentrations (WSIC; range: 2.3–39.9 $\mu g\,m^{-3}$) with higher and lower average values during the winter and summer months, respectively. SO_4^{2-} ions were predominant among anions, while NH_4^+ was a major contributor among cations throughout the season. The estimated pH of FPM from the forward and reverse modes exhibits a moderate correlation for winter and summer samples. The estimated pH of FPM is largely regulated by SO_4^{2-} content and strongly depends on the relative ambient humidity, particularly in the forward mode. Major sources of FPM assessed based on Positive matrix factorization (PMF) and air-mass back trajectory analyses demonstrate the dominance of natural sources (sea salt and dust) during summer months, anthropogenic sources in winter months and mixed sources during the post-monsoon season.

Keywords: aerosol pH; aerosol water content; aerosol sources; Arabian Sea; aerosol chemistry

1. Introduction

The ability of FPM ($PM_{2.5}$, particulate matter with 2.5 and less than 2.5 μm aerodynamic diameter) to absorb considerable amounts of water has significant effects on its physical and chemical characteristics, as well as on atmospheric processes and human health [1,2]. The chemical composition, relative humidity (RH), and temperature of FPM govern its pH and liquid water content (LWC), which are in chemical equilibrium with the surrounding water vapor. FPM, or $PM_{2.5}$, is mostly composed of secondary inorganic aerosol (SIA) [2] and its production in the atmosphere involves a set of precursor gases (emitted from anthropogenic and biogenic sources) which undergo gas-to-particle conversion [3–7]. Several studies have substantiated that meteorological factors (temperature, wind speed, relative humidity and mixing height of boundary layer) and gas-phase precursors are key determinants in the formation of SIA [8–11]. SIAs, including sulfate (SO_4^{2-}), nitrate (NO_3^-) and ammonium (NH_4^+), typically dominate water-soluble ionic species in

$PM_{2.5}$ and have been reported to account for more than 90% of WSIC (water-soluble ionic concentration) in continental as well as coastal regions [7,12–14]. Among these SIAs, SO_4^{2-} is the dominant acidic component of FPM [13,15,16], and it is mostly responsible for its acidity [17–19].

Globally, FPM pH is in the acidic range, mainly due to the ubiquitous abundance of acidic species like H_2SO_4, HNO_3, and HCl [19,20]. However, NH_3 gas, which is present in the form of NH_4^+ ions in particulate matter, being abundant in the atmosphere, shifts the pH towards the alkaline side. The concentration of strong acids, as well as the ambient temperature and RH, controls the NH_3 partitioning, resulting in the dependence of pH on the chemical composition of particles [21,22]. To understand the relation among pH, gaseous precursors, and meteorological conditions, the concentration of SIA and LWC are taken into account and analyzed. There have been significant efforts in the continental region to understand the relationship between SIA formation and estimated pH [19,23]. Sharma et al. [23] suggested that underestimation of LWC during periods of high SIA and RH can potentially affect the characteristics of heterogeneous chemistry on the FPM surface.

Marine FPM plays an important role in the Earth's radiation budget [24]; it can contribute to acid deposition [25] and strongly influence cloud properties over the oceans. In coastal regions, SIA has a strong effect on hygroscopicity and can influence $PM_{2.5}$ levels, which control particle acidity that governs FPM formation, their fate and its impact on the oceanic ecosystem [9,26,27]. The acidic species (sulfate and nitrate) formed in the atmosphere get mixed with mineral FPM and can decrease its pH to such levels that Fe and P containing minerals become more labile [28,29]. Particle acidity affects FPM concentrations, chemical composition and global biogeochemical cycles by controlling the solubility—and thus increasing the bioavailability of limiting nutrients that are transported via the atmospheric pathway to the marine ecosystem [30–36]. FPM acidity directly affects the deposition and lifetime of many compounds in the atmosphere through its influence on the gas–particle partitioning of semi-volatile species, including NH_3, nitric acid (HNO_3), and organic acids [37–40]. Coastal and remote marine environments are generally dominated by seawater-derived natural fine particles; however, the outflow of continental air masses in favorable meteorological conditions can have strong impacts on their composition and characteristics. These continental air masses have been affected by a wide range of anthropogenic (fossil fuels, biomass burning, and industry) and natural (dust and sea salt) emissions [29]. While there have been various studies on the relationship between SIA formation and FPM pH as well as meteorological indices over the continent [7,41–43], no studies have been reported on particle acidity behavior from the coastal region, particularly from the Indian coastal region. The relationship between precursor gaseous pollutants, SIA formation with the aerosol pH and LWC, as well as their seasonal variability, have implications for nutrient availability and their deposition in the surface oceanic waters.

Thermodynamic models, such as ISORROPIA-II and E-AIM have been extensively used to estimate aerosol pH and LWC using their inorganic composition [44,45]. Aerosols absorb water as a function of the relative humidity of air due to the deliquescent behavior of chemical species, which determine their composition [27,29,45]. In this study, we have used ISORROPIA-II to calculate the acidity and LWC of $PM_{2.5}$ based on their chemical composition. We have analyzed the chemical composition of $PM_{2.5}$ collected on depth filters using a high-volume sampler during three different seasons between December 2017 and February 2019. This study is further complemented by source identification using PMF and air mass back trajectory (AMBT) analyses, which are used to assess the relative contribution from various sources, which can impact the variation of FPM pH and LWC. Finally, statistical methods were employed to analyze the relative influence of meteorological conditions, gas-phase precursors, and SIA on particle acidity to understand the nature of the particle and its impact on the coastal region.

2. Methodology

2.1. Study Site

The FPM collection site is located in Goa (15.45° N, 73.20° E) on the west coast of India on the campus of the CSIR-National Institute of Oceanography (CSIR-NIO). Details of the sampling site and prevailing meteorology are discussed in Kaushik et al. [12]. A total of 109 $PM_{2.5}$ samples were collected using a high-volume sampler (TISCH Environmental, Cleves, OH, USA). All samples were collected for 24 h, at an average flow rate of 1.1 $m^3 \cdot min^{-1}$ on PALLFLEX™ (New York, NY, USA) Tissuquartz filters (8″ × 10″). A few samples, between April 2018 and May 2018, were collected on Whatman-41 cellulose filters (20 × 25 cm) (Marlborough, MA, USA) using the same high-volume samplers. Prior to sample collection, quartz filters were conditioned in an oven at a temperature of 200 °C for 3–4 h. The detailed methodology for the sample analyses in the laboratory is discussed by Kaushik et al. [12]. Briefly, a piece of filter was leached with deionized water (Milli-Q; specific resistivity > 18.2 MΩ-cm) (Rahway, NJ, USA) following ultrasonication for 30 min. The water extract was subsequently filtered through a PVDF syringe filter with a pore size of 0.2 μm and then transferred to a pre-conditioned polypropylene bottle. This solution was analyzed for cations (Na^+, NH_4^+, K^+, Mg^{2+}, and Ca^{2+}) and anions (Cl^-, NO_3^-, and SO_4^{2-}) using a Thermo scientific ion chromatography system (Dionex ICS 5000) (Waltham, MA, USA). Merck (Rahway, NJ, USA) multi-element standard was used for standard preparation by suitably diluting it. Calibration for each ion was performed before starting the analyses, and fresh standards were prepared before analyses. Along with samples, field blanks were also extracted and analyzed using a similar methodology as that of aerosol samples. Details of filter blank and corrections are given in Kaushik et al. [12]. The reproducibility in the analytical data for the measured concentration is within 5% based on the repeat analysis of a number of samples and standards. In this study, concentrations of SO_4^{2-}, NO_3^-, and NH_4^+ in $PM_{2.5}$ were used to quantify the presence of SIA in the coastal region of the northern Indian Ocean.

2.2. Datasets Used and Their Sources

In thermodynamic equilibrium with gas-phase precursors, ISORROPIA-II estimates the composition and phase state of K^+, Ca^{2+}, Mg^{2+}, NH_4^+, Na^+, SO_4^{2-}, NO_3^-, Cl^-, and H_2O in FPM. Chemical and meteorological data are also required as input for calculations [45]. The inorganic ions measured by the Thermo Scientific Ion Chromatography equipment (Dionex ICS 5000) are inputs to the ISORROPIA-II for our analysis. Meteorological data were also acquired using the Automatic Weather System (AWS) installed on the CSIR-National Institute of Oceanography's roof (~56 m above sea level [12]). The gas phase measurement was also conducted at CSIR-NIO with a Continuous Ambient Air Quality Monitoring Station (CAAQMS) [46]. The gas-phase dataset (daily SO_2, NO_2 and NH_3 concentrations) used in the study has been collected from CAAQMS on an hourly to daily basis, and their monthly average has been used as an input value.

2.3. ISORROPIA-II and pH Estimation

ISORROPIA-II is a thermodynamic equilibrium model that uses observed particulate species to predict the equilibrium partitioning of species (Na^+, SO_4^{2-}, NO_3^-, Cl^-, Ca^{2+}, Mg^{2+}, NH_4^+, Na^+ and K^+) among the particle phase for reverse mode and with its corresponding gas phase for forward mode in order to determine the concentration of H^+ ion in fine particles [44,47]. Model inputs include species-specific gas and particle concentrations, as well as meteorological parameters (RH and temperature) that influence pH [34]. ISORROPIA-II was used in this study in forward and reverse modes, using the "metastable" phase state. In forward mode, the equilibrium partitioning is calculated using the total concentration of different species (gas and particle) as well as relative humidity and temperature as input, whereas, in reverse mode, the thermodynamic composition is predicted solely using the aerosol chemical composition [45].

In this study, the ISORROPIA-II has been used for pH prediction, validation, and uncertainty analysis following the study reported by Guo et al. [47] and Weber et al. [19], during the Southern Oxidant and Aerosol Study (SOAS). FPM pH is defined as

$$pH = -\log_{10} H^+_{aq} = -\log_{10} \frac{1000 H^+_{air}}{W_i + W_o} \simeq -\log_{10} \frac{1000 H^+_{air}}{W_i}$$

where, H^+_{aq} (mole L^{-1}) is the hydronium ion concentration in particle liquid water, H^+_{air} ($\mu g \ m^{-3}$) is the hydronium ion concentration per unit volume of air, and W_i and W_o ($\mu g \ m^{-3}$) are particle water concentrations associated with inorganic and organic species, respectively. Guo et al. [45] have reported that pH predicted only by W_i was fairly accurate; pH was consistently 0.15–0.23 units lower than the pH predicted by the total water particle concentrations ($W_i + W_o$) ($R^2 = 0.97$). ISORROPIA-II computes the liquid water particle content in equilibrium with the ambient relative humidity and considers the non-idealities between all dissolved major ions in the solution. In the calculations of pH, the hydrogen ion activity is assumed to be unity [19,28].

2.4. Aerosol Ion Balance and Molar Ratio

The acid-base equilibrium of aerosol is assessed using ion balance calculations. The AE (anion equivalent) and CE (cations equivalent) ratios can be used to determine atmospheric aerosol acidity [48,49]. The particulate anion and cations equivalent were calculated as follows [48–50]:

$$AE = \frac{[SO_4^{2-}]}{48} + \frac{[NO_3^-]}{62} + \frac{[Cl^-]}{35.5}$$

$$CE = \frac{[NH_4^+]}{18} + \frac{[Ca^{2+}]}{20} + \frac{[K^+]}{39} + \frac{[Mg^{2+}]}{12} + \frac{[Na^+]}{23}$$

where, Na^+, SO_4^{2-}, NO_3^-, Cl^-, Ca^{2+}, Mg^{2+}, NH_4^+, and K^+ represent the respective ion mass concentrations in $PM_{2.5}$ samples. An AE/CE (anion/cation) ratio greater than unity indicates acidic condition, while those less than 1 indicate a more alkaline nature of FPM [32,48,49], although thermodynamic modelling and source apportionment reveal a more complicated relationship. For an accurate and unbiased pH calculation, both gas and FPM phase concentrations are needed; however, when some uncertainty can be tolerated, or the level of pH bias is known, aerosol ionic composition alone can be quite informative for determining the pH [45].

The molar ratio is the proportion of the total molar concentration of observed inorganic cations to the total molar concentration of observed inorganic anions:

$$Molar \ ratio = \frac{\sum (cation)}{\sum (anion)}$$

The molar ratio has been used as a proxy for acidity in various studies, with smaller ratios corresponding to particles associated with the highest levels of acidity (lowest pH) [49]. For fully neutralized FPM, molar ratios that generate a charge balance (i.e., equivalence ratios of one or more) are assumed [33].

2.5. PMF and AMBT

In this study, we have used PMF for the quantitative determination of contribution from various sources (local vis-à-vis long-range transport) to the ambient aerosols. These results are further corroborated by the 7 days AMBTs derived from the Hybrid Single Particle Lagrangian Integrated Trajectory Model (HYSPLIT; http://ready.arl.noaa.gov/HYSPLIT.php (accessed on 13 November 2022) [51], arriving in Goa at 500 m above ground level every 24 h. PMF is a valuable approach for determining probable particulate matter source contributions. PMF gives factor scores with minimal rotational ambiguity and rigorously nonnegative factor loading. With the known error predictions of the components

of the data matrix used to compute the weights, PMF utilizes a weighted least squares fit. PMF proposes a solution that minimizes an object function, Q, for each observation depending on uncertainties [52]. The calculated uncertainties for each data value are critical to PMF's effectiveness. Uncertainty estimate is a valuable approach for reducing the weight of missing and below-detection-limit data in the solution, as well as accounting for source profile variability. The concentration values were used directly for the observed datasets, and their uncertainty estimations were specified as 10% of the mass concentration [53]. Values below the limit of detection were substituted with half of the detection limit values, with 5/6 of the detection limit values as overall uncertainty. The geometric mean of the measurements was used to replace missing values, and the associated uncertainties were set to four times these geometric mean values [54].

3. Results and Discussion

The WSIC mass concentration for the $PM_{2.5}$ was highest for the winter season ranging from 10.1–39.9 $\mu g\ m^{-3}$ with a mean value of 19.6 $\pm$ 5.8 $\mu g\ m^{-3}$ followed by the post-monsoon season (range: 2.3–29.0 $\mu g\ m^{-3}$; mean: 14.4 $\pm$ 8.0 $\mu g\ m^{-3}$) and the summer season (mean: 12.9 $\pm$ 7.3; range: 0.8–31.6 $\mu g\ m^{-3}$). Relatively large variability in the WSIC is observed during the post-monsoon as well as summer months. The large variation in post-monsoon season is possibly attributed to significant variability in sources (i.e., marine and continental mixed wind parcels) contributing to the FPM mass. Moreover, the contribution of mineral dust (from the middle-east desert region) and sea salt (from the marine region) led to the larger variability during summer, which is also evident from the air-mass back trajectory analyses (discussed in more detail in later sections) [12].

3.1. Seasonal Variability in Ion Balance, Aerosol Acidity and LWC

The mass concentrations of the water-soluble inorganic cations and anions present in the samples were used for the thermodynamic calculations. The collected FPMs were found to be dominated by SIA (SO_4^{2-}, NH_4^+, NO_3^-), and their percentage contribution to the FPM mass ranged from 23 to 96%. The non-volatile cations (NVCs, i.e., the sum of Na^+, Ca^{2+}, K^+, and Mg^{2+}, mean = 1.24 $\pm$ 0.89 $\mu g\ m^{-3}$) constitute around 14% (range: 1–30%) of total WSIC. The correlation plot between the total anion and total cation (in equivalent units) along the 1:1 line is shown in Figure 1. Few samples were found to fall towards the cation axis, indicating a case of cation excess, which may be due to the lack of measurement of bicarbonate and organic anions [12]. A very significant correlation (r^2 = 0.94; $p < 0.005$) was found between the concentration of measured cations and anions, and the equivalent ratio of anion-to-cation was also found to be very close to unity (winter: 0.82 to 1.20, summer: 0.64 to 1.16, and post-monsoon: 0.80 to 1.19). The majority of the samples had a negative ion balance (i.e., cations < anions) and thus, a lower pH value is expected, indicating the high acidity of the samples. A similar observation has been reported by Shi et al. [28] using observational datasets for different regions. The estimated pH using the forward mode ranged from −0.36 to 4.11, which showed a large spread in contrast to the pH estimated from the reverse mode (range: −0.36 to 2.2). In addition, the forward mode estimated pH was not found to be sensitive to the ion balance, which is mainly due to the fact that the forward mode calculations constitute additional constraints because of the partitioning of semi-volatile species. Nevertheless, the estimated pH (by either mode) was found to be on the lower side, depicting a highly acidic scenario.
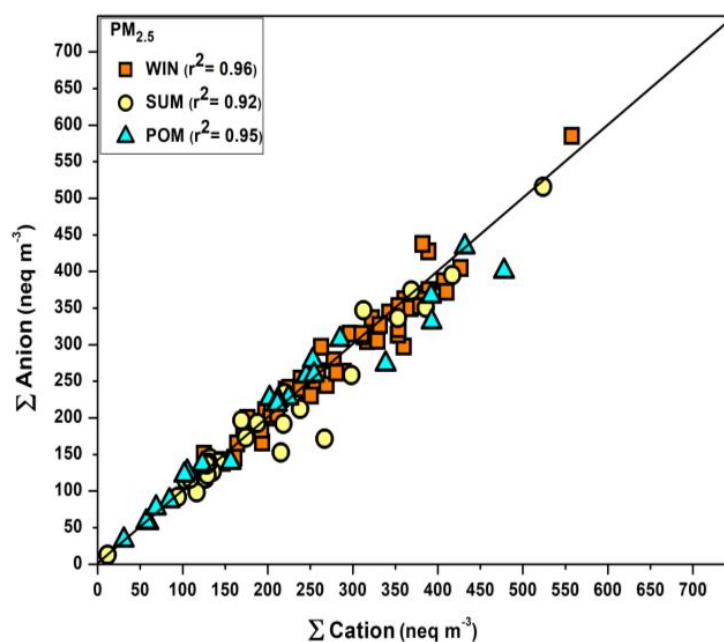
Figure 1. Correlation plot between total anion and total cation in equivalence units for aerosols collected in different seasons. (WIN = Winter, SUM = Summer, POM = Post-monsoon).

The seasonal variability in estimated aerosol pH using ISORROPIA-II (forward and reverse mode) is shown as a box plot in Figure 2a,b. The estimated pH in the forward and reverse modes ranged from -0.36 to 4.11 (mean $= 2.49 \pm 1.11$) and -0.36 to 2.2 (mean $= 1.02 \pm 0.46$), respectively. Relatively large seasonal variability was observed in pH estimated from the forward mode in contrast to the reverse mode, with higher values during summer and winter months. However, a relatively more acidic value was estimated during the post-monsoon months. Interestingly, the estimated pH in reverse mode for all months is comparable with those estimated for the post-monsoon month (forward mode). A large overestimation was observed for the estimated pH in the forward mode for the winter and summer months. This may be attributed to the uncertainty associated with the availability of gas-phase data. Due to the availability of simultaneous aerosol and gas-phase data, the forward-mode estimates were higher than the reverse-mode estimates. While analyzing the seasonal variations in the pH values of FPM, the role of air mass derived from different sources (anthropogenic versus natural dust/sea salt) is very important and its impact can be inferred from the AMBT analyses (discussed in a later section). Most of the FPM pH values were around 2–4, with only a small fraction, particularly during the post-monsoon season, having a pH of 2 or below based on bulk composition. The results from all three seasons indicated that aerosol pH changed considerably for a given group of meteorological conditions (temperature and RH). In addition to FPM pH, ISORROPIA-II was used to estimate the liquid water content (LWC) in PM$_{2.5}$ samples through forward and reverse mode, and their seasonal variation is displayed as box plots in Figure 2b. The LWC associated with the WSIC has varied from 7.1–593.9 (111.7 ± 121.2) µg m^{-3} and 0.66–227.5 (32.7 ± 38.3) µg m^{-3} in forward and reverse mode, respectively. The observed seasonal variability of LWC in reverse mode was found highest in winter with an average value of 42.4 ± 46.1 µg m^{-3}, followed by post-monsoon and summer with average values of 29.8 ± 28.7 µg m^{-3} and 15.6 ± 17.5 µg m^{-3}, respectively. However, in the forward mode, the concentration of LWC showed a higher degree of variation having average values of 155.8 ± 148.4 µg m^{-3}, 108.3 ± 135.1 µg m^{-3}, 59.5 ± 102.3 µg m^{-3} during winter, summer and post-monsoon, respectively. Both reverse and forward approaches forecast different FPM pH and LWC values. Despite significant quantities of gas-phase ammonia and high RH, the models in reverse mode predict very acidic conditions over extended periods. Furthermore, the models in reverse mode are extremely sensitive to measurement

uncertainty [55]. This statement is consistent with earlier reports that demonstrate that the use of FPM-gas inputs improves model performance significantly [33,45,56].
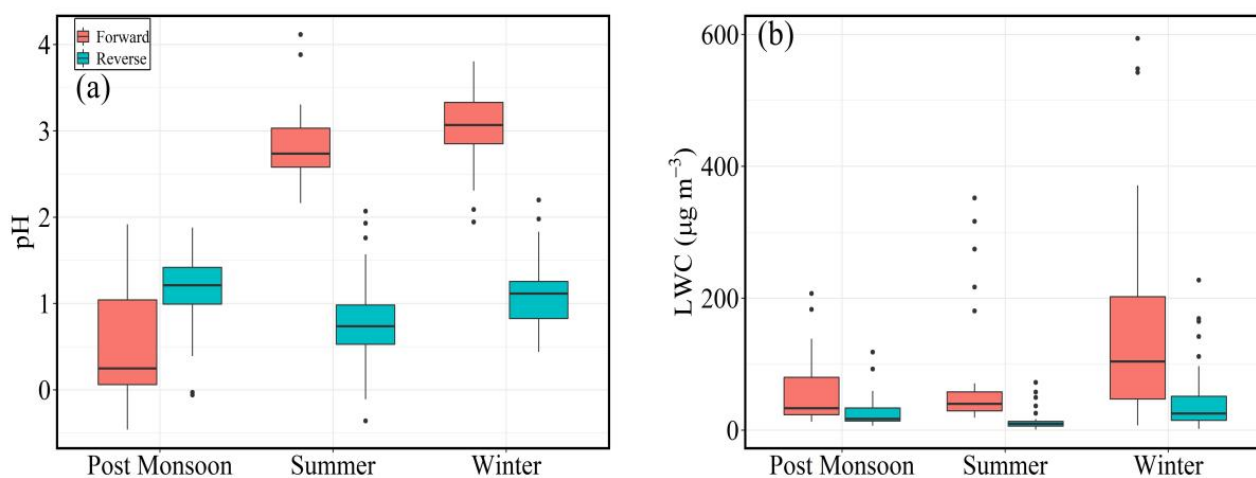

Figure 2. Box plots showing seasonal variability of (**a**) aerosol pH and (**b**) liquid water content of $PM_{2.5}$ estimated using forward and reverse during the study period at Goa.

The scatter plot between estimated pH for different seasons in forward and reverse mode is displayed in Figure 3a,b. Aerosol pH is overestimated in forward mode with a correlation ($r^2 = 0.26$; $p < 0.005$) observed for the summer and winter months samples. However, a relatively large scatter with under-estimated aerosol pH is found for the reverse mode for the post-monsoon samples.
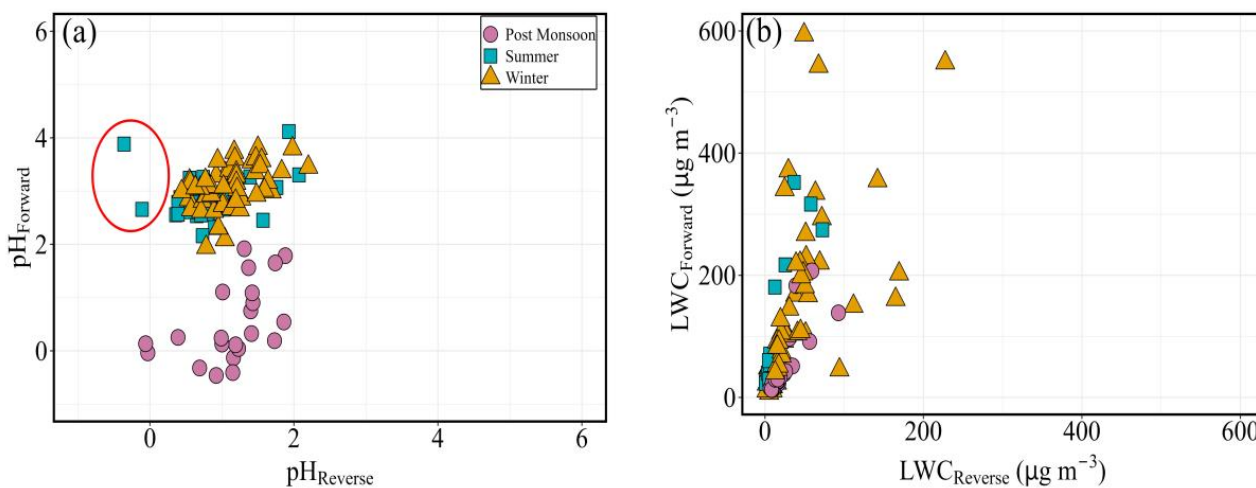

Figure 3. Correlation plots between estimated (**a**) aerosol pH and (**b**) liquid water content in forward and reverse mode of $PM_{2.5}$ during the study period at Goa. (outliers are in a circle and they are not used for correlation calculation).

We further assessed the relationship between the estimated pH and the RH associated with the samples, and the scatter plot between them is shown in Figure 4a,b. A very general increasing trend was observed between aerosol pH and relative humidity, which is more prominent in the forward mode in contrast to the reverse mode. This increase is shown in the summer and winter as well as the post-monsoon samples, although they have different slopes (Figure 4a). However, up to 80% RH, there is no substantial increase in pH in the reverse mode (Figure 4b); but, a rapid increase is displayed post 80% RH. This increasing trend is also nicely correlated with an increase in liquid water content (Figure 4b). In this study, a 24 h average of RH has been considered to get a single data point and

compared with the pH of FPM. There is significant diurnal variability expected for RH, so we attempted sensitivity analyses to assess the impact of varying RH on the pH of FPM. The variation in pH for FPM for all samples at different RH values is shown in Supplementary Material 1 (Figure S1). A high RH condition, which is a typical characteristic of a coastal site, enables aqueous-phase pathways for SO_2 oxidation to take place as the particulate matter takes up more water from the atmosphere. The atmospheric liquid water content increases by orders of magnitude when the atmosphere warms up during the day, followed by sea breezes; hence, the SO_2 aqueous-phase oxidation pathways play an important role in the formation of SO_4^{2-} FPM in this region. In addition, NH_4^+ concentration levels were not found to be significantly high and contributing to the neutralization of the acidity caused by the higher level of SO_4^{2-}, especially in the reverse mode. Furthermore, the mass concentrations of NO_3^-, Cl^- and non-volatile cations (Na^+, K^+, Ca^{2+}, Mg^{2+}) all combined together have a contribution of more than 6% to the total FPM mass, but they did not seem to affect the pH in the region as evident from the reverse mode calculations. Considering the forward mode runs, gaseous NH_3 was added to the NH_4^+ FPM, and its impact was found to result in higher values of pH. Coarsely, a 10-fold increase in the concentration of NH_3 is entailed to increase the pH by one unit, revealing an inherent consistency between much different FPM systems [47]. The results from both modes provide evidence that NH_4^+ or NH_3(g) availability is an important governing factor in stabilizing pH during the study period except in the post-monsoon season, while the contribution of NVCs was quite insignificant in decreasing FPM acidity throughout the study period. According to this finding, smaller concentrations of NH_4^+ are responsible for inconsistent alkalinity, which is a major factor in the NO_2 oxidation pathway to suppress SO_4^{2-} formation [47].
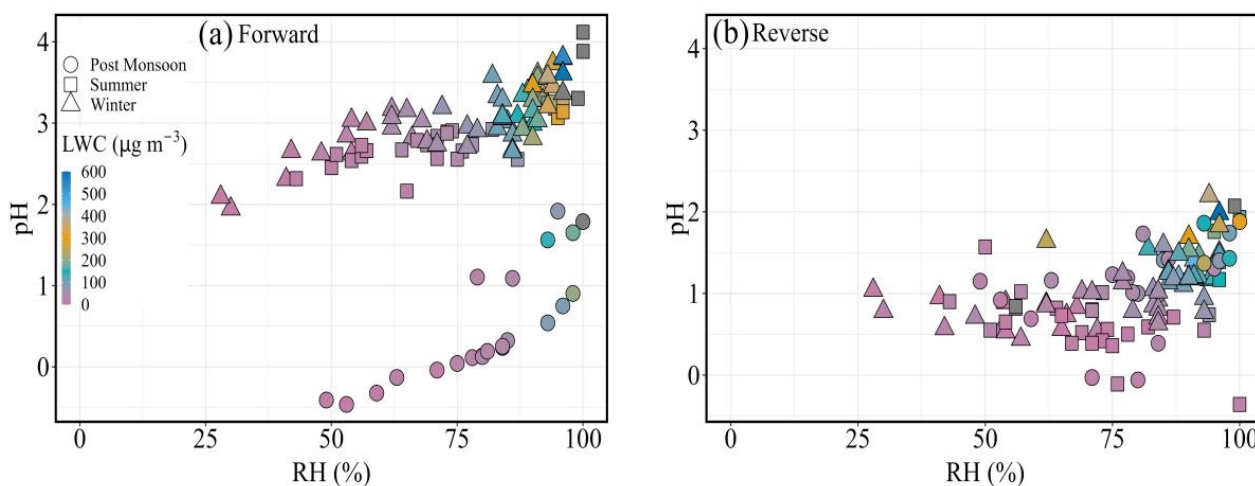

Figure 4. Relationship between aerosol pH and relative humidity at varying LWC in (**a**) forward and (**b**) reverse mode.

During the post-monsoon period, relatively lower pH values were observed because of the availability of high SO_4^{2-} even at considerable NH_4^+/NH_3 (g) and nitrate levels. Throughout this period, even when total ammonia is quite significant, the presence of high water content is found, and pH is low, although such occurrences are rare (e.g., the period following a sudden spike in the particulate matter) [50]. It is evident from Figure 5a that with an increase in NO_3^- and NH_4^+ concentrations, all considerable water is taken up, resulting in an increase in water content. The increased water content can provide a large FPM surface and volume, promoting secondary aerosol production and increasing SO_4^{2-} and NO_3^- generation as well as NH_4^+ aerosol partitioning [57,58].
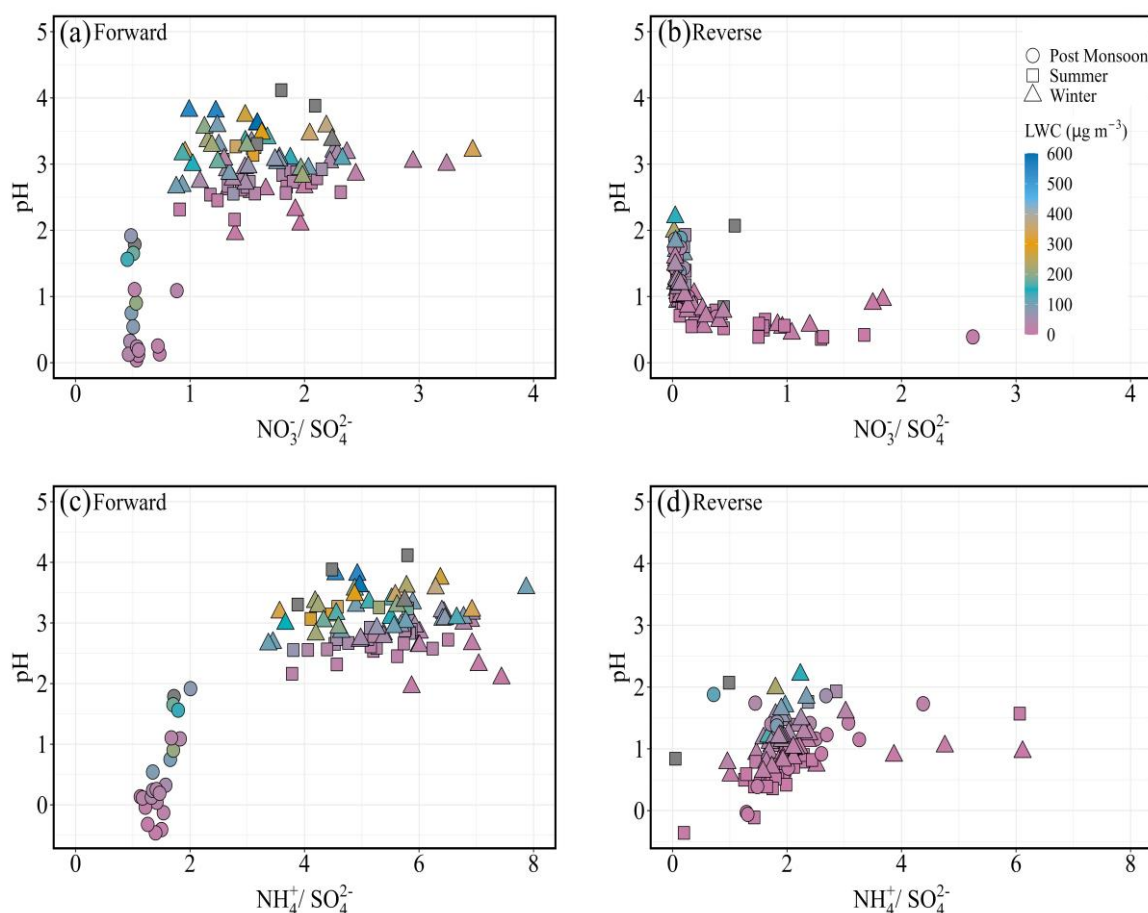
Figure 5. Aerosol pH as a function of (**a**) nitrate to sulfate molar ratio in forward mode; (**b**) nitrate to sulfate molar ratio in reverse mode; (**c**) ammonium to sulfate molar ratio in forward mode; (**d**) ammonium to sulfate molar ratio in reverse mode.

The molar ratio is widely used as a proxy for aerosol pH, similar to the ion balance, to assess the acidity of aerosols. Fully neutralized aerosol is considered to have a molar ratio that generates a charge balance (i.e., equivalency ratios) of unity or above, while decreasing cation/anion (NH_4^+/SO_4^{2-}) molar ratios are supposed to imply decreasing aerosol pH [49,59,60]. The molar ratio approach is based on the same data and assumptions that were used to determine the ion balance. As a result, the molar ratio technique suffers from many of the same drawbacks. Minor ionic species, such as crustal elements and dissociated organic acids, might dramatically influence the results if they are not included [61–65]. Considering the same assumptions and restrictions as above for the study data set, the ion balance method was found to follow the cation/anion molar ratio. Similarly, there was a good association between the NH_4^+/SO_4^{2-} molar ratio with forward mode aerosol pH ($r^2 = 0.63$) (Figure S2) estimates, whereas, in reverse mode, the correlation was poor. The molar ratio may reliably identify alkaline particles from acidic ones when the bulk of inorganic species (>95%) are considered; nevertheless, it cannot provide any assessment—even qualitative—of the degree of aerosol acidity [33]. The link between the molar ratio and estimated aerosol pH (with and without gas phase data) implies that relying solely on the molar ratio as a proxy for pH is not recommended; other measures (e.g., thermodynamic modelling) should be used to supplement the results.

3.2. FPM pH Response to NO_3^-, NH_4^+ and SO_4^{2-}

The NO_3^-/SO_4^{2-} and NH_4^+/SO_4^{2-} molar ratios were calculated to assess the response of pH to the molar concentrations of NO_3^-, SO_4^{2-}, and NH_4^+. Figure 5 displays

the variation of FPM pH (estimated in both modes) for the $PM_{2.5}$ samples as a function of the NO_3^-/SO_4^{2-} and NH_4^+/SO_4^{2-} ratio. The NO_3^-/SO_4^{2-} ratio showed an increasing a negative trend with the aerosol pH in forward mode (Figure 5a). However, a negative trend is observed for aerosol pH in the reverse run (Figure 5b). As the NO_3^-/SO_4^{2-} molar ratio increases and particles become gradually concentrated in NH_4NO_3, the pH of the aerosol increases [66]. The positive feedback between particle NO_3^- production and aerosol pH could be one of the reasons for such an increase [47]. Because of its strong hygroscopicity, nitrate also increases FPM water content (evident in Figure 5a,b), which lowers H^+ concentrations in the aqueous phase and increases aerosol pH. The greater the pH of the aerosol, the more enrichment of NO_3^- will occur [66]. These results show that nitrate formation via gas-to-particle conversion involving ammonia and nitric acid increases aerosol pH as the ratio of nitrate to sulfate increases. In contrast, as ammonia emissions are reduced, there will be a drop in aerosol pH associated with an increase in nitrate relative abundance [66]. A similar increase in the NO_3^-/SO_4^{2-} ratio has been reported from various parts of the world, including the United States and Canada [67–69]. As a result of this, $PM_{2.5}$ is increasingly becoming acidic, with a lower pH for the HSO_4^-/SO_4^{2-} system than the HNO_3/NO_3^- system [70].

Similar to the NO_3^-/SO_4^{2-} molar ratio, the NH_4^+/SO_4^{2-} ratio showed a significant increase in particle and gas phase data combined (Figure 5c,d). The ratio averaged 0.86 ± 0.34, with values ranging from 0.21 to 1.54. The higher acidity of the aerosol particles corresponds to the lower values of the NH_4^+/SO_4^{2-} ratio (Figure 5c,d). The ammonium–sulfate molar ratio (NH_4^+/SO_4^{2-}) should approach two when ammonia levels are high, with surplus ammonia staying in the gas phase. In deficits of NH_3, the aerosol should fully absorb it as ammonium (NH_4^+), with no considerable NH_3 remaining in the gas phase. Standard thermodynamic models suggest that when NH_3 levels are high, SO_4^{2-} aerosol will mostly consist of ammonium sulfate (($NH_4^+)_2SO_4$), with the NH_4^+/SO_4^{2-} ratio approaching two on a molar basis [71].

The correlations between NO_3^- and NH_4^+ at various SO_4^{2-} levels are shown in Figure 6. Pathak et al. (2009) found that the relationship between the molar ratios of NO_3^-/SO_4^{2-} and NH_4^+/SO_4^{2-} can give us evidence about NO_3^- particles formation since NH_4^+ particles tend to bond with SO_4^{2-} more than NO_3^- particles. The formation of particle NO_3^- through the reaction of HNO_3 with NH_3 is generally indicated by positive correlations between the molar ratios of NO_3^-/SO_4^{2-} and $NH_4^+ + SO_4^{2-}$ in NH_4^+ rich ($NH_4^+/SO_4^{2-} > 1$) conditions, whereas high levels of NO_3^- in NH_4^+ poor conditions may be formed through the hydrolysis of N_2O_5 on the FPM surface [59,72,73].
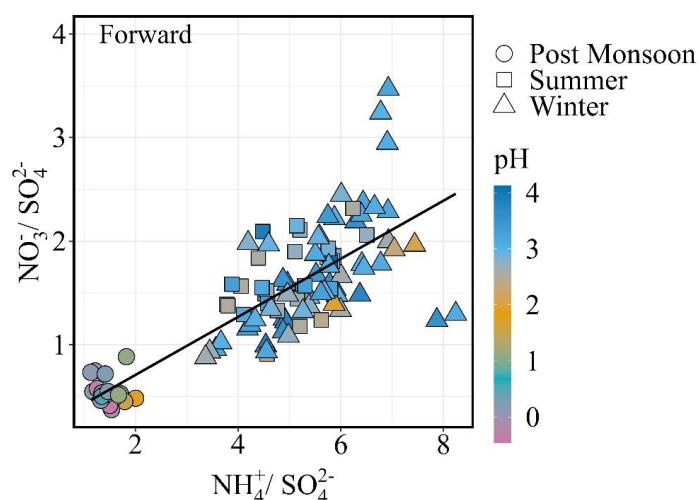

Figure 6. Nitrate to sulfate molar ratio as a function of ammonium to sulfate molar ratio.

We further evaluated the types of NH_4^+ present in the aerosol particle by analyzing the connection between NH_4^+ and SO_4^{2-} concentrations to identify NH_4^+ rich and NH_4^+

depleted (NH_4^+/SO_4^{2-} < 1) samples (Figure 7a,b). At NH_4^+ concentrations less than 10 μg m^{-3}, the slope of the regression line for NH_4^+ versus SO_4^{2-} was 0.27, showing that the majority of particle NH_4^+ was in the form of ammonium sulfate (i.e., $(NH_4)_2SO_4$) or Ammonium bisulfate (i.e., NH_4HSO_4) (Figure 7a,b). A sharper slope (0.94) was seen as NH_4^+ concentrations increased beyond 10 μg/m^3. It is clear from the increased slope and the dispersion of the data that a significant amount of NH_4^+ was coupled to anion species other than SO_4^{2-}, such as NO_3^-. A combination of SO_4^{2-} and NO_3^- appeared to collect more NH_4^+ than SO_4^{2-} alone at high NH_4^+ concentrations. This implies that once the NH_4^+/SO_4^{2-} molar ratio rises above 0.2, NH_4^+ exceeds the quantity necessary for SO_4^{2-} neutralization. The higher slope, together with scattered data points, shows that a significant percentage of NH_4^+ was coupled to anion species other than SO_4^{2-}, such as NO_3^-. The relative abundance of NO_3^- increases linearly with increasing NH_4^+/SO_4^{2-} molar ratio in NH_4^+ rich samples. This suggests that the NO_3^- particle is strongly linked to the production of ammonium nitrate (i.e., NH_4NO_3).
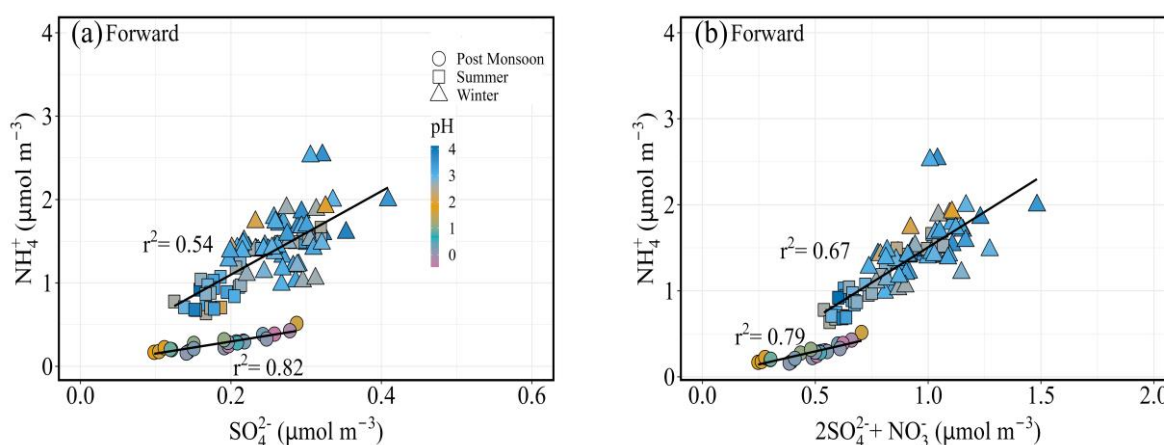

Figure 7. Ammonium concentration as a function of sulfate (**a**) and the sum of sulfate and nitrate (**b**) concentration of PM$_{2.5}$ samples.

3.3. Source Contribution Using PMF and AMBT

We have attempted to apportion sources of WSIC using PMF for the overall study duration to substantiate the role of various sources contributing to the inorganic concentration corresponding to every measured sample. Initially, an unconstrained PMF analysis was carried out with various solutions ranging from 2–9 factors and then their factor mass spectrum were assessed. Further, the solution with optimal factors (7 factors) was used to run PMF again with seven different seeds, and after examining the Q_{true}/Q_{exp} values, residuals, factor profiles and the results of bootstrap runs, the optimal solution was chosen [74]. On the basis of the factor profiles (Figure 8), the contribution of all factors except one was determined to be about equivalent. The dominating factor contributed the most to SO_4^{2-} (76.6%), which is mainly formed by gas-to-particle conversion processes from its primary precursor SO_2; nonetheless, it also contributed to Mg^{2+}. As SO_4^{2-} was most prominent in this component, it is important to note that it may also be formed from Dimethyl sulfide (DMS) mainly derived from biogenic emissions from surface ocean water [75]. In addition, local/regional sources and long-range transport of anthropogenic pollutants can potentially contribute to this coastal location [12]. The fresh sea salt factor was the second most contributing factor, distinguished by its substantial contribution to Cl^- (65.6%) and Na^+ (20.1%), which is an important signal for sea salt FPM. NH_4^+ (8.3%), Ca^{2+} (4.6%), and NO_3^- (2%) were some other minor contributors to this source. Following the fresh sea salt factor, the most contributing factor contained a high amount of Na^+ and Mg^{2+}. Given that Cl^- in sea salt is actively depleted by gaseous HNO_3 resulting in the formation of non-volatile $NaNO_3$, the absence of Cl^- and presence of NO_3^- imply that this component represents aged sea salt combined with secondary inorganic FPMs. Due to

sea salt's chemical reactivity with acids, the primary distinction between fresh and aged sea salt was the substitution of Cl^- for NO_3^- [76,77]. The factor apportioning to the dust source accounts for approximately 16% of the total $PM_{2.5}$. The considerable contribution of this source factor to crustal elements such as Ca^{2+} (20%) in this study identifies the factor as dust.
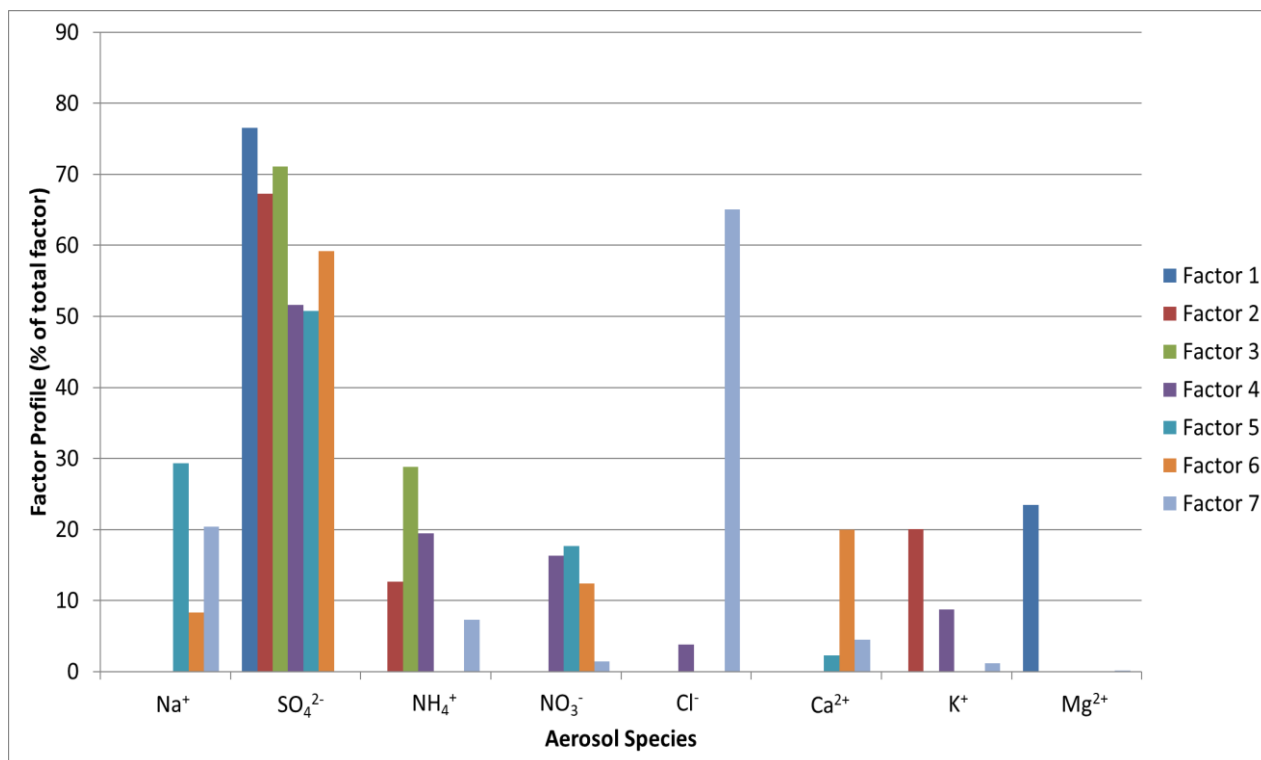

Figure 8. Relative contribution of various factors representing potential sources of water-soluble ionic species in aerosols collected at the study site.

Figure 9 shows daily as well as seasonal variation of contribution by each factor, respectively. On average, the contribution of the SO_4^{2-} factor was highest (51.6%) to the total WSIC, followed by the NVC source (18.5%), Cl^- (10.4%), NH_4^+ (10.6%), NO_3^- (9.2%). In winter, the absolute contribution ($\mu g\ m^{-3}$) was higher from each source factor than in the summer and post-monsoon periods. The percentage contributions (%) of the three seasons showed different patterns and were mainly dominated by SO_4^{2-} among all the SIA. It is worth noticing that the concentration of SO_4^{2-} was found to contribute the highest to $PM_{2.5}$ during the winter season than in the other two seasons. This is possibly due to long-range transport from the Indo-Gangetic Plains (IGP), which is also supported by the air mass back-trajectory analysis (AMBT) shown in Figure 10. It is evident from the AMBT analyses that the marine air parcel is dominant during the summer season (Figure 10). Moreover, SO_4^{2-} is high during summer, which can be attributed to the oxidation of Dimethyl sulfide (DMS) in the marine region, primarily from marine plankton, as well as via anthropogenic sources. On the basis of these findings, concentration-AMBT maps were created to identify sources that contribute to PMF components. The AMBTs during summer and post-monsoon seasons were mostly derived from the desert region, which are potential sources of mineral dust. High sulfate content during post-monsoon months associated with low pH and vice-versa during summer and winter months indicate a potential role of sources in impacting the pH and LWC of the aerosols.
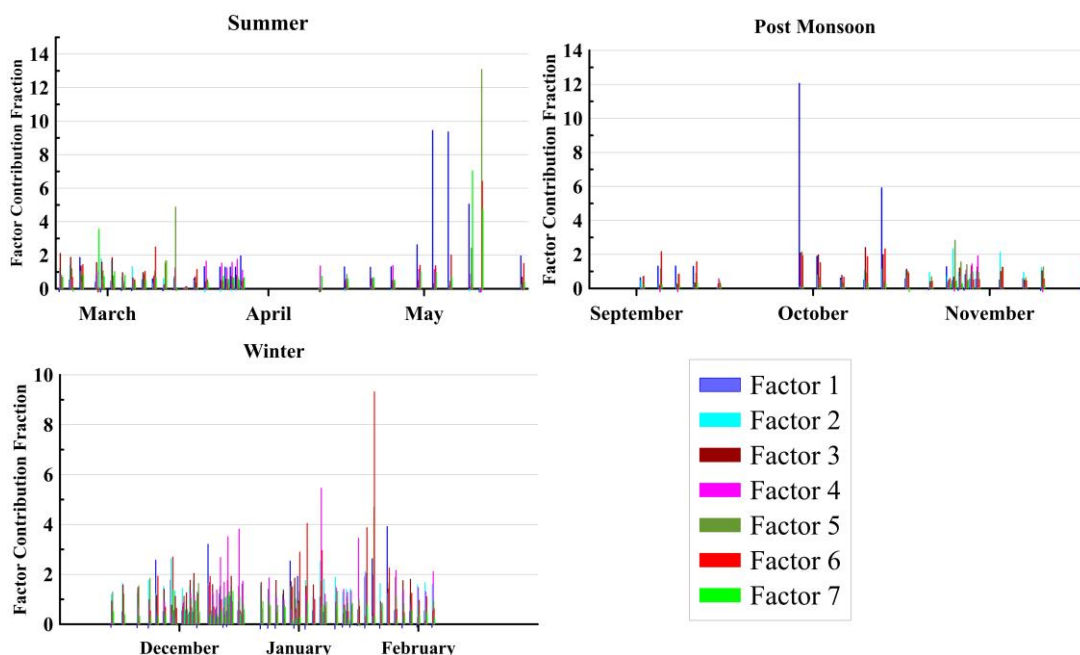
Figure 9. Seasonal variation of factor profile of aerosol species and their fractional contribution in different aerosol samples. Major dominant factors are factors 1, 2 and 3, which have been identified as sulfate-rich, sea salt and dust-dominated, respectively (see text for details).
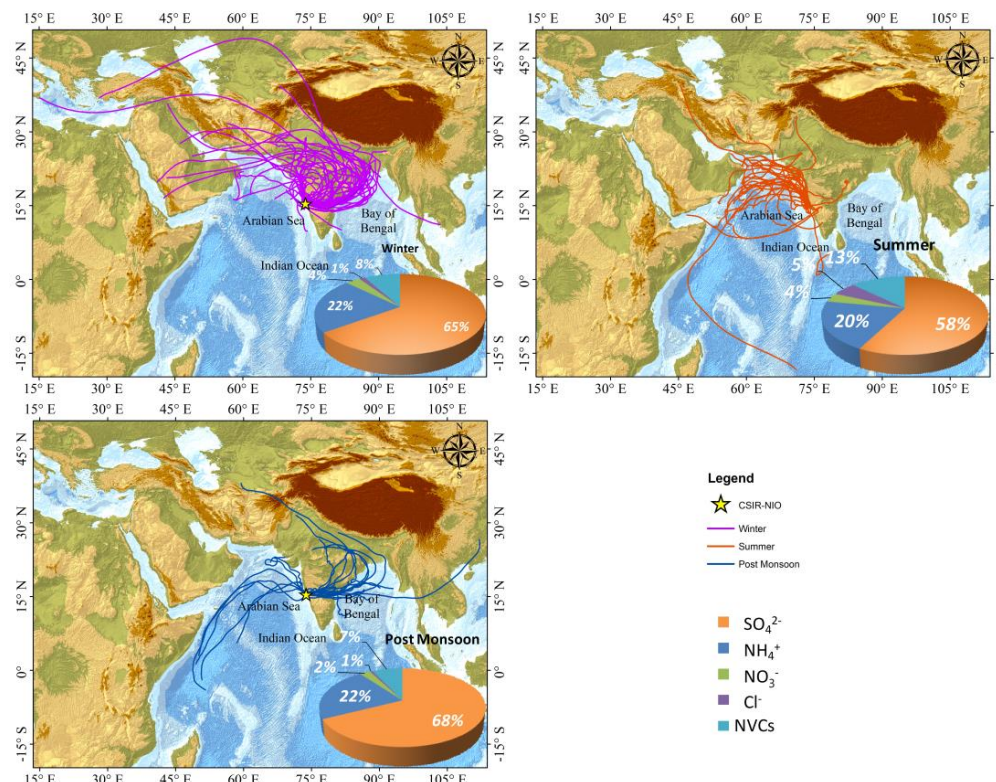

Figure 10. Seven-day Air Mass Back Trajectories ending at the sampling site at an altitude of 500 m.

4. Conclusions

This study provided the seasonal variability in the pH of FPM at a coastal location in the northeast Arabian Sea. Aerosol pH was estimated using particulate matter ionic composition as well as gas phase measurements at the study site. Relatively large seasonal variability was observed in the pH estimated from the forward mode, in contrast to the

reverse mode, with higher values during post-monsoon compared to summer and winter. Higher acidic aerosols during the post-monsoon season were associated with lower aerosol LWC (59.5 ± 102.2 µg m^{-3}) and vice versa for summer and winter. Our result suggests that equilibrium models with gas, as well as particulate phase input, can more accurately predict H$^+$ ions and aerosol pH. It is also found that the variation in aerosol pH was not significantly impacted by the small variation in relative humidity and, thus, LWC. SO$_4^{2-}$ is found to dominate the WSIC and is one of the controlling factors for high acidity over the study region. Source identification revealed air parcels originated primarily from the maritime region during summer, indicating the presence of DMS (from the phytoplankton) as a major contributor of SO$_4^{2-}$; however, anthropogenic emissions from local/regional sources as well as long-range transport contribute to sulfate during winter and post-monsoon months. This study has regional as well as global implications, especially with respect to the availability of macro and micronutrients and their impact on the biogeochemical processes pertaining to the Oceanic environment in a changing climate scenario.

Supplementary Materials: The following supporting information can be downloaded at: https://www.mdpi.com/article/10.3390/atmos14020259/s1, Figure S1: Variation of Aerosol pH for different ranges of RH (%) in Sensitivity Analysis; Figure S2: Aerosol pH as a function of ammonium to sulfate molar ratio in forward mode.

Author Contributions: A.K. and S.S.G. conceived the idea. A.K. designed and conceptualized the research. A.K. and G.S. planned the work and set up of Thermodynamic model ISORROPIA-II with the help of S.S.G. A.K. and G.S. have done processing of aerosol data and run the model. G.S. performed data interpretation with support from A.K. and S.S.G. G.S. wrote the draft of the manuscript under the mentorship of A.K. with critical edits and inputs form A.K.S. and G.B. and comments from S.S.G. All the co-authors discussed the results and commented on the manuscript. All authors have read and agreed to the published version of the manuscript.

Data Availability Statement: The data presented in this study are available on request from the corresponding author. The data are not publicly available as it is a part of thesis study of a student.

Conflicts of Interest: The authors declare no conflict of interest.

References

1. Khlystov, A.; Stanier, C.O.; Takahama, S.; Pandis, S.N. Water Content of Ambient Aerosol during the Pittsburgh Air Quality Study. *J. Geophys. Res. Atmos.* **2005**, *110*. [CrossRef]
2. Fu, X.; Wang, S.; Chang, X.; Cai, S.; Xing, J.; Hao, J. Modeling Analysis of Secondary Inorganic Aerosols over China: Pollution Characteristics, and Meteorological and Dust Impacts. *Sci. Rep.* **2016**, *6*, 35992. [CrossRef] [PubMed]
3. Clement, C. Gas-to-Particle Conversion in the Atmosphere: I. Evidence from Empirical Atmospheric Aerosols. *Atmos. Environ.* **1999**, *33*, 475–487. [CrossRef]
4. Gunthe, S.S.; Liu, P.; Panda, U.; Raj, S.S.; Sharma, A.; Darbyshire, E.; Reyes-Villegas, E.; Allan, J.; Chen, Y.; Wang, X.; et al. Enhanced Aerosol Particle Growth Sustained by High Continental Chlorine Emission in India. *Nat. Geosci.* **2021**, *14*, 77–84. [CrossRef]
5. Chapter 10: Gas-to-Particle Conversion | Engineering360. Available online: https://www.globalspec.com/reference/77570/203279/chapter-10-gas-to-particle-conversion (accessed on 16 November 2022).
6. Kulmala, M.; Kerminen, V.-M.; Petäjä, T.; Ding, A.J.; Wang, L. Atmospheric Gas-to-Particle Conversion: Why NPF Events Are Observed in Megacities? *Faraday Discuss.* **2017**, *200*, 271–288. [CrossRef] [PubMed]
7. Behera, S.N.; Sharma, M. Reconstructing Primary and Secondary Components of PM$_{2.5}$ Composition for an Urban Atmosphere. *Aerosol Sci. Technol.* **2010**, *44*, 983–992. [CrossRef]

8. Sudheer, A.K.; Rengarajan, R. Time-Resolved Inorganic Chemical Composition of Fine Aerosol and Associated Precursor Gases over an Urban Environment in Western India: Gas-Aerosol Equilibrium Characteristics. *Atmos. Environ.* **2015**, *109*, 217–227. [CrossRef]

9. Wang, H.; Ding, J.; Xu, J.; Wen, J.; Han, J.; Wang, K.; Shi, G.; Feng, Y.; Ivey, C.E.; Wang, Y.; et al. Aerosols in an Arid Environment: The Role of Aerosol Water Content, Particulate Acidity, Precursors, and Relative Humidity on Secondary Inorganic Aerosols. *Sci. Total Environ.* **2019**, *646*, 564–572. [CrossRef]

10. Tie, X.; Huang, R.-J.; Cao, J.; Zhang, Q.; Cheng, Y.; Su, H.; Chang, D.; Pöschl, U.; Hoffmann, T.; Dusek, U.; et al. Severe Pollution in China Amplified by Atmospheric Moisture. *Sci. Rep.* **2017**, *7*, 15760. [CrossRef]

11. Han, B.; Zhang, R.; Yang, W.; Bai, Z.; Ma, Z.; Zhang, W. Heavy Haze Episodes in Beijing during January 2013: Inorganic Ion Chemistry and Source Analysis Using Highly Time-Resolved Measurements from an Urban Site. *Sci. Total Environ.* **2016**, *544*, 319–329. [CrossRef]

12. Kaushik, A.; Kumar, A.; Aswini, M.A.; Panda, P.P.; Shukla, G.; Gupta, N.C. Seasonal Variation in Chemical Composition of Size-Segregated Aerosols Over the Northeastern Arabian Sea. *Front. Environ. Sci.* **2021**, *8*, 619174. [CrossRef]

13. Kumari, P.; Toshniwal, D. Impact of Lockdown Measures during COVID-19 on Air Quality—A Case Study of India. *Int. J. Environ. Health Res.* **2022**, *32*, 503–510. [CrossRef] [PubMed]

14. Devi, N.L.; Kumar, A.; Yadav, I.C. PM10 and PM2.5 in Indo-Gangetic Plain (IGP) of India: Chemical Characterization, Source Analysis, and Transport Pathways. *Urban Clim.* **2020**, *33*, 100663. [CrossRef]

15. Ghosh, A.; Patel, A.; Rastogi, N.; Sharma, S.K.; Mandal, T.K.; Chatterjee, A. Size-Segregated Aerosols over a High Altitude Himalayan and a Tropical Urban Metropolis in Eastern India: Chemical Characterization, Light Absorption, Role of Meteorology and Long Range Transport. *Atmos. Environ.* **2021**, *254*, 118398. [CrossRef]

16. Acharja, P.; Ali, K.; Ghude, S.D.; Sinha, V.; Sinha, B.; Kulkarni, R.; Gultepe, I.; Rajeevan, M.N. Enhanced Secondary Aerosol Formation Driven by Excess Ammonia during Fog Episodes in Delhi, India. *Chemosphere* **2022**, *289*, 133155. [CrossRef] [PubMed]

17. Ding, J.; Zhao, P.; Su, J.; Dong, Q.; Du, X.; Zhang, Y. Aerosol PH and Its Driving Factors in Beijing. *Atmos. Chem. Phys.* **2019**, *19*, 7939–7954. [CrossRef]

18. Gao, J.; Wei, Y.; Shi, G.; Yu, H.; Zhang, Z.; Song, S.; Wang, W.; Liang, D.; Feng, Y. Roles of RH, Aerosol PH and Sources in Concentrations of Secondary Inorganic Aerosols, during Different Pollution Periods. *Atmos. Environ.* **2020**, *241*, 117770. [CrossRef]

19. Weber, R.J.; Guo, H.; Russell, A.G.; Nenes, A. High Aerosol Acidity despite Declining Atmospheric Sulfate Concentrations over the Past 15 Years. *Nat. Geosci.* **2016**, *9*, 282–285. [CrossRef]

20. Pye, H.O.T.; Nenes, A.; Alexander, B.; Ault, A.P.; Barth, M.C.; Clegg, S.L.; Collett, J.L., Jr.; Fahey, K.M.; Hennigan, C.J.; Herrmann, H.; et al. The Acidity of Atmospheric Particles and Clouds. *Atmos. Chem. Phys.* **2020**, *20*, 4809–4888. [CrossRef]

21. Zheng, M.; Xu, K.; Yuan, L.; Chen, N.; Cao, M. Fine Particle PH and Its Impact on PM2.5 Control in a Megacity of Central China. *Aerosol Air Qual. Res.* **2022**, *22*, 210394. [CrossRef]

22. Battaglia, M.A., Jr.; Balasus, N.; Ball, K.; Caicedo, V.; Delgado, R.; Carlton, A.G.; Hennigan, C.J. Urban Aerosol Chemistry at a Land–Water Transition Site during Summer—Part 2: Aerosol PH and Liquid Water Content. *Atmos. Chem. Phys.* **2021**, *21*, 18271–18281. [CrossRef]

23. Sharma, M.; Kishore, S.; Tripathi, S.N.; Behera, S.N. Role of Atmospheric Ammonia in the Formation of Inorganic Secondary Particulate Matter: A Study at Kanpur, India. *J. Atmos. Chem.* **2007**, *58*, 1–17. [CrossRef]

24. Forster, P.; Ramaswamy, V.; Artaxo, P.; Berntsen, T.; Betts, R.; Fahey, D.W.; Haywood, J.; Lean, J.; Lowe, D.C.; Myhre, G.R.; et al. Changes in Atmospheric Constituents and in Radiative Forcing. *Clim. Chang.* **2007**. Available online: https://archive.ipcc.ch/publications_and_data/ar4/wg1/en/ch2.html (accessed on 13 November 2022).

25. Larssen, T.; Lydersen, E.; Tang, D.; He, Y.; Gao, J.; Liu, H.; Duan, L.; Seip, H.M.; Vogt, R.D.; Mulder, J.; et al. Acid Rain in China. *Environ. Sci. Technol.* **2006**, *40*, 418–425. [CrossRef] [PubMed]

26. Squizzato, S.; Masiol, M.; Brunelli, A.; Pistollato, S.; Tarabotti, E.; Rampazzo, G.; Pavoni, B. Factors Determining the Formation of Secondary Inorganic Aerosol: A Case Study in the Po Valley (Italy). *Atmos. Chem. Phys. Discuss.* **2012**, *12*, 16377–16406. [CrossRef]

27. Wu, L.; Wang, Y.; Li, L.; Zhang, G. Acidity and Inorganic Ion Formation in PM2.5 Based on Continuous Online Observations in a South China Megacity. *Atmos. Pollut. Res.* **2020**, *11*, 1339–1350. [CrossRef]

28. Shi, G.; Xu, J.; Peng, X.; Xiao, Z.; Chen, K.; Tian, Y.; Guan, X.; Feng, Y.; Yu, H.; Nenes, A.; et al. PH of Aerosols in a Polluted Atmosphere: Source Contributions to Highly Acidic Aerosol. *Environ. Sci. Technol.* **2017**, *51*, 4289–4296. [CrossRef]

29. Bougiatioti, A.; Nikolaou, P.; Stavroulas, I.; Kouvarakis, G.; Weber, R.; Nenes, A.; Kanakidou, M.; Mihalopoulos, N. Particle Water and PH in the Eastern Mediterranean: Source Variability and Implications for Nutrient Availability. *Atmos. Chem. Phys.* **2016**, *16*, 4579–4591. [CrossRef]

30. Meskhidze, N.; Chameides, W.L.; Nenes, A.; Chen, G. Iron Mobilization in Mineral Dust: Can Anthropogenic SO_2 Emissions Affect Ocean Productivity? *Geophys. Res. Lett.* **2003**, 30. [CrossRef]

31. Meskhidze, N.; Chameides, W.L.; Nenes, A. Dust and Pollution: A Recipe for Enhanced Ocean Fertilization? *J. Geophys. Res. Atmos.* **2005**, 110. [CrossRef]

32. Nenes, A.; Krom, M.D.; Mihalopoulos, N.; Van Cappellen, P.; Shi, Z.; Bougiatioti, A.; Zarmpas, P.; Herut, B. Atmospheric Acidification of Mineral Aerosols: A Source of Bioavailable Phosphorus for the Oceans. *Atmos. Chem. Phys.* **2011**, *11*, 6265–6272. [CrossRef]

33. Hennigan, C.J.; Izumi, J.; Sullivan, A.P.; Weber, R.J.; Nenes, A. A Critical Evaluation of Proxy Methods Used to Estimate the Acidity of Atmospheric Particles. *Atmos. Chem. Phys.* **2015**, *15*, 2775–2790. [CrossRef]

34. Fang, T.; Guo, H.; Zeng, L.; Verma, V.; Nenes, A.; Weber, R.J.; Nenes, A.; Weber, R.J. Highly Acidic Ambient Particles, Soluble Metals, and Oxidative Potential: A Link between Sulfate and Aerosol Toxicity. *Environ. Sci. Technol.* **2017**, *51*, 2611–2620. [CrossRef]

35. Mahowald, N. Aerosol Indirect Effect on Biogeochemical Cycles and Climate. *Science* **2011**, *334*, 794–796. [CrossRef] [PubMed]

36. Baker, A.R.; Kanakidou, M.; Nenes, A.; Myriokefalitakis, S.; Croot, P.L.; Duce, R.A.; Gao, Y.; Guieu, C.; Ito, A.; Jickells, T.D.; et al. Changing Atmospheric Acidity as a Modulator of Nutrient Deposition and Ocean Biogeochemistry. *Sci. Adv.* **2021**, *7*, eabd8800. [CrossRef] [PubMed]

37. Ahrens, L.; Harner, T.; Shoeib, M.; Lane, D.A.; Murphy, J.G. Improved Characterization of Gas–Particle Partitioning for Per- and Polyfluoroalkyl Substances in the Atmosphere Using Annular Diffusion Denuder Samplers. *Environ. Sci. Technol.* **2012**, *46*, 7199–7206. [CrossRef]

38. Keene, W.C.; Pszenny, A.A.P.; Maben, J.R.; Stevenson, E.; Wall, A. Closure Evaluation of Size-Resolved Aerosol PH in the New England Coastal Atmosphere during Summer. *J. Geophys. Res. Atmos.* **2004**, *109*. [CrossRef]

39. Rengarajan, R.; Sudheer, A.K.; Sarin, M.M. Wintertime PM2.5 and PM10 Carbonaceous and Inorganic Constituents from Urban Site in Western India. *Atmos. Res.* **2011**, *102*, 420–431. [CrossRef]

40. Sudheer, A.K.; Rengarajan, R.; Sheel, V. Secondary Organic Aerosol over an Urban Environment in a Semi–Arid Region of Western India. *Atmos. Pollut. Res.* **2015**, *6*, 11–20. [CrossRef]

41. Pay, M.T.; Jiménez-Guerrero, P.; Baldasano, J.M. Assessing Sensitivity Regimes of Secondary Inorganic Aerosol Formation in Europe with the CALIOPE-EU Modeling System. *Atmos. Environ.* **2012**, *51*, 146–164. [CrossRef]

42. Norazman, N.H.; Khan, M.F.; Ramanathan, S.; Mustapa Kama Shah, S.; Mohd Jani, S.J.; Joy, K.S.; Islam, K.N.; Jeba, F.; Salam, A.; Yoshida, O.; et al. Influence of Monsoonal Driving Factors on the Secondary Inorganic Aerosol over Ambient Air in Dhaka. *ACS Earth Space Chem.* **2021**, *5*, 2517–2533. [CrossRef]

43. Sun, X.; Wang, H.; Guo, Z.; Lu, P.; Song, F.; Liu, L.; Liu, J.; Rose, N.L.; Wang, F. Positive Matrix Factorization on Source Apportionment for Typical Pollutants in Different Environmental Media: A Review. *Environ. Sci. Process. Impacts* **2020**, *22*, 239–255. [CrossRef] [PubMed]

44. Fountoukis, C.; Nenes, A. ISORROPIA II: A computationally efficient thermodynamic equilibrium model for K^+–Ca^{2+}–Mg^{2+}–NH^{4+}–Na^+–SO_4^{2-}–NO_3^-–Cl^-–H_2O aerosols. *Atmos. Chem. Phys.* **2007**, *7*, 4639–4659. [CrossRef]

45. Guo, H.; Xu, L.; Bougiatioti, A.; Cerully, K.M.; Capps, S.L.; Hite, J.R.; Carlton, A.G.; Lee, S.-H.; Bergin, M.H.; Ng, N.L.; et al. Fine-Particle Water and PH in the Southeastern United States. *Atmos. Chem. Phys.* **2015**, *15*, 5211–5228. [CrossRef]

46. Beig, G.; Sahu, S.K.; Singh, V.; Tikle, S.; Sobhana, S.B.; Gargeva, P.; Ramakrishna, K.; Rathod, A.; Murthy, B.S. Objective Evaluation of Stubble Emission of North India and Quantifying Its Impact on Air Quality of Delhi. *Sci. Total Environ.* **2020**, *709*, 136126. [CrossRef] [PubMed]

47. Guo, H.; Liu, J.; Froyd, K.D.; Roberts, J.M.; Veres, P.R.; Hayes, P.L.; Jimenez, J.L.; Nenes, A.; Weber, R.J. Fine Particle PH and Gas–Particle Phase Partitioning of Inorganic Species in Pasadena, California, during the 2010 CalNex Campaign. *Atmos. Chem. Phys.* **2017**, *17*, 5703–5719. [CrossRef]

48. Zhang, T.; Cao, J.J.; Tie, X.X.; Shen, Z.X.; Liu, S.X.; Ding, H.; Han, Y.M.; Wang, G.H.; Ho, K.F.; Qiang, J.; et al. Water-Soluble Ions in Atmospheric Aerosols Measured in Xi'an, China: Seasonal Variations and Sources. *Atmos. Res.* **2011**, *102*, 110–119. [CrossRef]

49. Kerminen, V.-M.; Hillamo, R.; Teinilä, K.; Pakkanen, T.; Allegrini, I.; Sparapani, R. Ion Balances of Size-Resolved Tropospheric Aerosol Samples: Implications for the Acidity and Atmospheric Processing of Aerosols. *Atmos. Environ.* **2001**, *35*, 5255–5265. [CrossRef]

50. Shi, G.; Xu, J.; Shi, X.; Liu, B.; Bi, X.; Xiao, Z.; Chen, K.; Wen, J.; Dong, S.; Tian, Y.; et al. Aerosol PH Dynamics During Haze Periods in an Urban Environment in China: Use of Detailed, Hourly, Speciated Observations to Study the Role of Ammonia Availability and Secondary Aerosol Formation and Urban Environment. *J. Geophys. Res. Atmos.* **2019**, *124*, 9730–9742. [CrossRef]

51. Polissar, A.V.; Hopke, P.K.; Paatero, P.; Malm, W.C.; Sisler, J.F. Atmospheric Aerosol over Alaska: 2. Elemental Composition and Sources. *J. Geophys. Res. Atmos.* **1998**, *103*, 19045–19057. [CrossRef]

52. Pekey, H.; Pekey, B.; Arslanbaş, D.; Bozkurt, Z.B.; Doğan, G.; Tuncel, G. Source Apportionment of Personal Exposure to Fine Particulate Matter and Volatile Organic Compounds Using Positive Matrix Factorization. *Water Air Soil Pollut.* **2012**, *224*, 1403. [CrossRef]

53. Kim, E.; Larson, T.V.; Hopke, P.K.; Slaughter, C.; Sheppard, L.E.; Claiborn, C. Source Identification of PM2.5 in an Arid Northwest U.S. City by Positive Matrix Factorization. *Atmos. Res.* **2003**, *66*, 291–305. [CrossRef]

54. Song, S.; Gao, M.; Xu, W.; Shao, J.; Shi, G.; Wang, S.; Wang, Y.; Sun, Y.; McElroy, M.B. Fine-Particle PH for Beijing Winter Haze as Inferred from Different Thermodynamic Equilibrium Models. *Atmos. Chem. Phys.* **2018**, *18*, 7423–7438. [CrossRef]

55. Fountoukis, C.; Nenes, A.; Sullivan, A.; Weber, R.; Van Reken, T.; Fischer, M.; Matías, E.; Moya, M.; Farmer, D.; Cohen, R.C. Thermodynamic Characterization of Mexico City Aerosol during MILAGRO 2006. *Atmos. Chem. Phys.* **2009**, *9*, 2141–2156. [CrossRef]

56. Behera, S.N.; Sharma, M.; Aneja, V.P.; Balasubramanian, R. Ammonia in the Atmosphere: A Review on Emission Sources, Atmospheric Chemistry and Deposition on Terrestrial Bodies. *Environ. Sci. Pollut. Res.* **2013**, *20*, 8092–8131. [CrossRef]

57. Liu, M.; Song, Y.; Zhou, T.; Xu, Z.; Yan, C.; Zheng, M.; Wu, Z.; Hu, M.; Wu, Y.; Zhu, T. Fine Particle PH during Severe Haze Episodes in Northern China. *Geophys. Res. Lett.* **2017**, *44*, 5213–5221. [CrossRef]

58. He, K.; Zhao, Q.; Ma, Y.; Duan, F.; Yang, F.; Shi, Z.; Chen, G. Spatial and Seasonal Variability of PM$_{2.5}$ Acidity at Two Chinese Megacities: Insights into the Formation of Secondary Inorganic Aerosols. *Atmos. Chem. Phys.* **2012**, *12*, 1377–1395. [CrossRef]

59. Huang, K.; Zhuang, G.; Wang, Q.; Fu, J.S.; Lin, Y.; Liu, T.; Han, L.; Deng, C. Extreme Haze Pollution in Beijing during January 2013: Chemical Characteristics, Formation Mechanism and Role of Fog Processing. *Atmos. Chem. Phys. Discuss.* **2014**, *14*, 7517–7556. [CrossRef]

60. Cao, J.; Tie, X.; Dabberdt, W.F.; Jie, T.; Zhao, Z.; An, Z.; Shen, Z.; Feng, Y. On the Potential High Acid Deposition in Northeastern China. *J. Geophys. Res. Atmos.* **2013**, *118*, 4834–4846. [CrossRef]

61. Jacobson, M.Z. Isolating Nitrated and Aromatic Aerosols and Nitrated Aromatic Gases as Sources of Ultraviolet Light Absorption. *J. Geophys. Res. Atmos.* **1999**, *104*, 3527–3542. [CrossRef]

62. Trebs, I.; Metzger, S.; Meixner, F.X.; Helas, G.; Hoffer, A.; Rudich, Y.; Falkovich, A.H.; Moura, M.A.L.; da Silva, R.S., Jr.; Artaxo, P.; et al. The NH4$^+$-NO3$^-$-Cl$^-$-SO$_4$$^{2-}$-H$_2$O Aerosol System and Its Gas Phase Precursors at a Pasture Site in the Amazon Basin: How Relevant Are Mineral Cations and Soluble Organic Acids? *J. Geophys. Res. Atmos.* **2005**, *110*. [CrossRef]

63. Ziemba, L.D.; Fischer, E.; Griffin, R.J.; Talbot, R.W. Aerosol Acidity in Rural New England: Temporal Trends and Source Region Analysis. *J. Geophys. Res. Atmos.* **2007**, *112*. [CrossRef]

64. Moya, M.; Castro, T.; Zepeda, M.; Baez, A. Characterization of Size-Differentiated Inorganic Composition of Aerosols in Mexico City. *Atmos. Environ.* **2003**, *37*, 3581–3591. [CrossRef]

65. Cao, Y.; Zhang, Z.; Xiao, H.; Xie, Y.; Liang, Y.; Xiao, H. How Aerosol PH Responds to Nitrate to Sulfate Ratio of Fine-Mode Particulate. *Environ. Sci. Pollut. Res.* **2020**, *27*, 35031–35039. [CrossRef] [PubMed]

66. Cheng, I.; Zhang, L. Long-Term Air Concentrations, Wet Deposition, and Scavenging Ratios of Inorganic Ions, HNO$_3$, and SO$_2$ and Assessment of Aerosol and Precipitation Acidity at Canadian Rural Locations. *Atmos. Chem. Phys.* **2017**, *17*, 4711–4730. [CrossRef]

67. Lawal, A.S.; Guan, X.; Liu, C.; Henneman, L.R.F.; Vasilakos, P.; Bhogineni, V.; Weber, R.J.; Nenes, A.; Russell, A.G. Linked Response of Aerosol Acidity and Ammonia to SO2 and NOx Emissions Reductions in the United States. *Environ. Sci. Technol.* **2018**, *52*, 9861–9873. [CrossRef]

68. Murphy, J.G.; Gregoire, P.K.; Tevlin, A.G.; Wentworth, G.R.; Ellis, R.A.; Markovic, M.Z.; VandenBoer, T.C. Observational Constraints on Particle Acidity Using Measurements and Modelling of Particles and Gases. *Faraday Discuss.* **2017**, *200*, 379–395. [CrossRef]

69. Craig, R.L.; Nandy, L.; Axson, J.L.; Dutcher, C.S.; Ault, A.P. Spectroscopic Determination of Aerosol pH from Acid–Base Equilibria in Inorganic, Organic, and Mixed Systems. *J. Phys. Chem. A* **2017**, *121*, 5690–5699. [CrossRef]

70. Pandis, S.N.; Seinfeld, J.H. Sensitivity Analysis of a Chemical Mechanism for Aqueous-Phase Atmospheric Chemistry. *J. Geophys. Res. Atmos.* **1989**, *94*, 1105–1126. [CrossRef]

71. Pathak, R.K.; Wu, W.S.; Wang, T. Summertime PM$_{2.5}$ Ionic Species in Four Major Cities of China: Nitrate Formation in an Ammonia-Deficient Atmosphere. *Atmos. Chem. Phys.* **2009**, *9*, 1711–1722. [CrossRef]

72. Tian, S.; Pan, Y.; Wang, Y. Ion Balance and Acidity of Size-Segregated Particles during Haze Episodes in Urban Beijing. *Atmos. Res.* **2018**, *201*, 159–167. [CrossRef]

73. Sun, Y.L.; Wang, Z.F.; Du, W.; Zhang, Q.; Wang, Q.Q.; Fu, P.Q.; Pan, X.L.; Li, J.; Jayne, J.; Worsnop, D.R. Long-Term Real-Time Measurements of Aerosol Particle Composition in Beijing, China: Seasonal Variations, Meteorological Effects, and Source Analysis. *Atmos. Chem. Phys.* **2015**, *15*, 10149–10165. [CrossRef]

74. Keller, M.D. Dimethyl Sulfide Production and Marine Phytoplankton: The Importance of Species Composition and Cell Size. *Biol. Oceanogr.* **1989**, *6*, 375–382. [CrossRef]

75. Adachi, K.; Buseck, P.R. Changes in Shape and Composition of Sea-Salt Particles upon Aging in an Urban Atmosphere. *Atmos. Environ.* **2015**, *100*, 1–9. [CrossRef]

76. Kotchenruther, R.A. The Effects of Marine Vessel Fuel Sulfur Regulations on Ambient PM2.5 at Coastal and near Coastal Monitoring Sites in the U.S. *Atmos. Environ.* **2017**, *151*, 52–61. [CrossRef]

77. Corral, A.F.; Dadashazar, H.; Stahl, C.; Edwards, E.-L.; Zuidema, P.; Sorooshian, A. Source Apportionment of Aerosol at a Coastal Site and Relationships with Precipitation Chemistry: A Case Study over the Southeast United States. *Atmosphere* **2020**, *11*, 1212. [CrossRef]